Optical properties of titanium-doped lithium niobate from time-dependent density-functional theory

Michael Friedrich,* W. G. Schmidt, and Arno Schindlmayr
Department Physik, Universität Paderborn, 33095 Paderborn, Germany

Simone Sanna
Institut für Theoretische Physik, Justus-Liebig-Universität Gießen, Heinrich-Buff-Ring 16, 35392 Gießen, Germany
(Received 8 May 2017; published 1 August 2017)

The optical properties of pristine and titanium-doped $LiNbO_3$ are modeled from first principles. The dielectric functions are calculated within time-dependent density-functional theory, and a model long-range contribution is employed for the exchange-correlation kernel in order to account for the electron-hole binding. Our study focuses on the influence of substitutional titanium atoms on lithium sites. We show that an increasing titanium concentration enhances the values of the refractive indices and the reflectivity.

DOI: 10.1103/PhysRevMaterials.1.034401

I. INTRODUCTION

Lithium niobate ($LiNbO_3$, LN) combines pronounced ferroelectric, pyroelectric, piezoelectric, electro-optical, acousto-optical, and nonlinear optical properties and so finds applications in numerous technical devices. For instance, LN waveguides are ideally suited for low-loss integrated linear and nonlinear quantum photonics. Further tuning of the physical properties is achieved by the indiffusion of a variety of metals. Titanium indiffusion is particularly promising, because Ti doping increases both the ordinary and the extraordinary refractive index [1], thus enabling low-loss optical waveguiding for both transverse electric (TE) and transverse magnetic (TM) polarization (parallel and perpendicular to the surface of the waveguide structure, respectively). Furthermore, Ti ions do not directly increase the photorefractive sensitivity of LN. Little is known about the microscopic properties of Ti, Fe, and other (optical) dopants in LN, however. Electron paramagnetic resonance (EPR) and electron-nuclear double resonance (ENDOR) in reduced samples reveal signals attributed to Ti^{3+} ions on Nb sites [2,3], while x-ray absorption spectroscopy, such as extended x-ray absorption fine structure (EXAFS) and x-ray absorption near-edge structure (XANES), indicates Ti^{4+} ions on regular Li sites [4] (see Fig. 1).

The theoretical knowledge of the structural and electronic properties of point defects in LN lags far behind the technological applications. Most of the information about intrinsic defects and common dopants date back to the works of Donnerberg and co-workers [5], which rely on semiempirical potentials, whereas state-of-the-art investigations based on density-functional theory (DFT) are rare and not exhaustive [6–8]. The incorporation of Ti strongly affects the optical and electro-optical properties exploited in waveguides [9]. It has been speculated that the dependence of the ordinary refractive index on the Ti concentration is related to a concentration-dependent displacement of the Ti ions in the xy plane [10], but no conclusive evidence is available.

In this work, we focus on an atomistic understanding of optical waveguides and perform first-principles calculations for unreduced LN samples incorporating only Ti_{Li} substitutionals. We do not consider Ti^{3+} ions on Nb sites, because these introduce electronic states inside the optical band gap that lead to absorption patterns in the optical spectra and are therefore undesirable in optical waveguides. We determine the structure of the Ti_{Li} substitutionals and analyze their impact on the dielectric function, refractive indices, and reflectivity. Theoretical spectroscopy based on the independent-particle approximation does not satisfactorily describe the experimentally measured onset and the shape of the optical absorption in LN [11]. More accurate simulations make use of many-body perturbation theory and the solution of the Bethe-Salpeter equation (BSE) for coupled electron-hole excitations, which is computationally very demanding. Therefore, in theoretical calculations, only stoichiometric LN (SLN) has been dealt with exhaustively until now [11,12]. Here we strive to overcome these limitations by employing time-dependent density-functional theory (TDDFT) [13] together with the long-range contribution (LRC) for the exchange-correlation kernel [14] to account for the electron-hole binding. This kernel incorporates the correct behavior in the optical limit of small wave vectors known from the BSE and has been successfully applied to a variety of semiconductors and wide-band-gap insulators [15]. It thus allows us to compute dielectric functions for realistic structures without neglecting many-body effects. An alternative to the long-range contribution, the so-called bootstrap approach, expresses the kernel in terms of the dielectric function. Different variants, which also exhibit the correct long-range behavior and contain no adjustable parameters, have been empirically derived [16–18]. For the purpose of comparison, we consider both the LRC and the bootstrap kernel in this work. In this way, reliable excited-state calculations for Ti-doped LN ultimately become possible.

II. COMPUTATIONAL METHOD

In this work we focus on single Ti_{Li} point defects. Our calculations are performed in charged supercells, so that the substitutionals always stay in the Ti_{Li}^{4+} charge state. Different titanium concentrations are simulated by choosing different supercell sizes. One Ti atom inside a $2 \times 2 \times 2$ supercell with 80 atoms or inside a $3 \times 3 \times 3$ supercell with 270 atoms yields a concentration of 1.16 or 0.35×10^{21}

*michael.friedrich@uni-paderborn.de

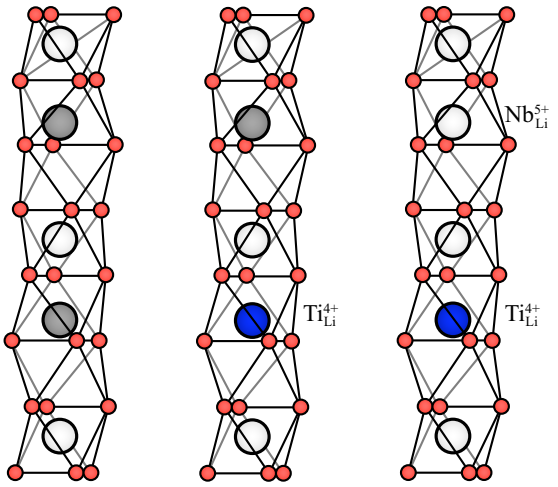

FIG. 1. Extrinsic defects in titanium-indiffused lithium niobate. The stoichiometric stacking sequence Nb (light gray)–vacancy–Li (dark gray) without defects is shown in (a). The small red circles indicate O atoms. In (b) the Ti^{4+}_{Li} substitutional defect (blue) is displayed. In (c) an additional Nb^{5+}_{Li} antisite defect is introduced into the material.

atoms per cm^3, respectively. Furthermore, a concentration of 1.05×10^{21} atoms per cm^3 can be simulated by placing three Ti_{Li} substitutionals into a $3 \times 3 \times 3$ supercell, where the titanium atoms are arranged to ensure a homogeneous distribution of defects.

Lithium niobate has a high density of intrinsic defects. It is commonly accepted that in congruent LN (CLN), the technologically relevant configuration, up to 5.9% of the Li^+ sites are occupied by niobium atoms (Nb^{5+}_{Li} antisites) [19]. For this reason, we carry out calculations for stoichiometric as well as congruent LN. Li:Nb ratios of 96% and 88% can be realized by introducing one Nb_{Li} antisite into our two differently sized supercells in addition to a Ti_{Li} antisite. In this way, titanium-doped SLN and CLN can be studied within the same framework.

Our ground-state calculations are performed within density-functional theory as implemented in the QUANTUM ESPRESSO package [20]. For the exchange-correlation energy we use the PBEsol parametrization [21], a generalized gradient approximation that reliably reproduces the experimental lattice constants of solids, including LN and related materials [22–24]. The electron-ion interaction is modeled using optimized norm-conserving Vanderbilt pseudopotentials [25], with the $1s$ and $2s$ orbitals of lithium, the $2s$ and $2p$ orbitals of oxygen, the $4s$, $4p$, $4d$, and $5s$ orbitals of niobium, and the $3s$, $3p$, $3d$, and $4s$ orbitals of titanium treated as valence electrons. For SLN, the plane-wave basis set is truncated at a cutoff energy of 1150 eV, and a Monkhorst-Pack [26] mesh of $4 \times 4 \times 4$ $\mathbf{k}$ points is used to converge the total energy of the system within 5×10^{-3} eV. To simulate the defects, we use supercells with 80 and 270 atoms. Reflecting the smaller Brillouin zone, the number of $\mathbf{k}$ points is reduced to $3 \times 3 \times 3$ and $2 \times 2 \times 2$, respectively, in this case. All atomic structures are relaxed with a convergence criterion of at least 0.01 eV/Å for the Hellmann-Feynman forces.

As the d electrons of transition metals typically exhibit a strong on-site Coulomb repulsion that is not described accurately by standard semilocal exchange-correlation functionals like PBEsol, we employ the DFT+U approach, which includes this effect explicitly. Here we use the formulation of Cococcioni *et al.* [27] and choose the value $U_{\text{eff}} = 4\,\text{eV}$ for titanium and niobium.

The excited-state calculations are carried out within TDDFT in the linear-response regime. The exchange-correlation kernel, defined as the functional derivative of the exchange-correlation potential with respect to the density, plays a central role in this framework. As its exact mathematical form is unknown, approximations are required for actual calculations. Our first choice here is the long-range contribution

$$f_{\mathbf{G}}^{\text{xc,LRC}}(\mathbf{q}) = -\frac{\alpha}{|\mathbf{q}+\mathbf{G}|^2}\,, \tag{1}$$

which is frequency independent and diagonal in the reciprocal lattice vectors $\mathbf{G}$. With this approximation, the dynamic linear density-response function is given by

$$\chi_{\mathbf{G}\mathbf{G}'}(\mathbf{q},\omega) = \chi^{\text{KS}}_{\mathbf{G}\mathbf{G}'}(\mathbf{q},\omega) + \sum_{\mathbf{G}''} \chi^{\text{KS}}_{\mathbf{G}\mathbf{G}''}(\mathbf{q},\omega) \times \left[v_{\mathbf{G}''}(\mathbf{q}) + f^{\text{xc}}_{\mathbf{G}''}(\mathbf{q})\right]\chi_{\mathbf{G}''\mathbf{G}'}(\mathbf{q},\omega)\,, \tag{2}$$

where $\mathbf{q}$ denotes the wave vector and ω the frequency of the incident light, $\chi^{\text{KS}}_{\mathbf{G}\mathbf{G}'}(\mathbf{q},\omega)$ is the linear Kohn-Sham independent-particle density-response function, optionally modified with a gap-opening scissors shift to account for electronic self-energy effects in a simplified way, and $v_{\mathbf{G}}(\mathbf{q}) = 4\pi/|\mathbf{q}+\mathbf{G}|^2$ is the Coulomb potential. The LRC is derived from the Bethe-Salpeter equation and ensures the correct qualitative behavior of $\chi_{\mathbf{G}\mathbf{G}'}(\mathbf{q},\omega)$ in the optical limit $\mathbf{q} \to \mathbf{0}$ [14]. It can be adjusted for a specific material through the parameter α. The LRC and the scissors shift of the Kohn-Sham eigenvalues can in fact be regarded as independent approximations for two distinct components of the exact exchange-correlation kernel [13]. The macroscopic dielectric function $\varepsilon(\omega)$ measured in optical absorption experiments is eventually obtained as

$$\varepsilon(\omega) = \lim_{\mathbf{q}\to\mathbf{0}} \frac{1}{1 + v_{\mathbf{0}}(\mathbf{q})\chi_{\mathbf{0}\mathbf{0}}(\mathbf{q},\omega)}\,. \tag{3}$$

The bootstrap approximation, considered as an alternative to the LRC in this work, is empirically derived and avoids adjustable parameters by expressing the exchange-correlation kernel in terms of the inverse dielectric function. In the optical limit, it is dominated by a divergent term of the same form as (1) with an explicitly given numerator that is inversely proportional to the macroscopic dielectric constant $\varepsilon_\infty = \varepsilon(\omega = 0)$ in the original formulation by Sharma *et al.* [16] (refered to BO in the following) or to the random-phase approximation thereof in the revised version (RBO) by Rigamonti *et al.* [17]. On the other hand, a fit of the values α that empirically lead to the best agreement with experimentally measured spectra for five materials, mostly sp^3-bonded semiconductors, also yields an inverse dependence $\alpha = 4.615/\varepsilon_\infty - 0.213$ on the macroscopic dielectric constant [15], reflecting the fact that an increased screening of the electron-hole attraction reduces the strength of excitonic effects. Despite their different origins, the bootstrap kernel and the LRC are thus expected to have

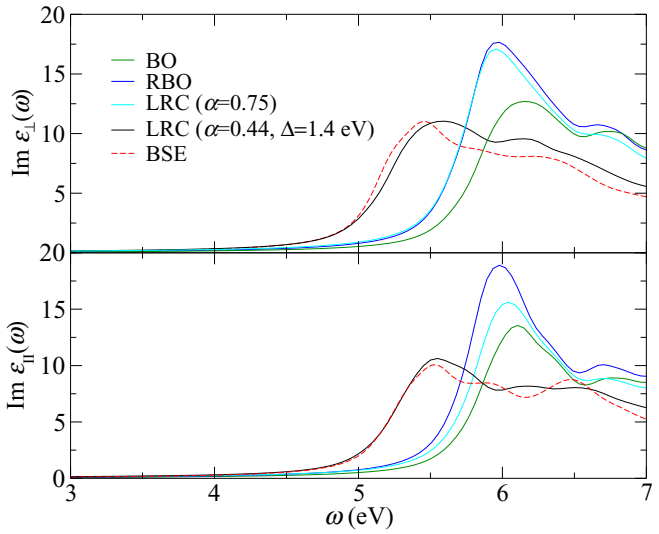

FIG. 2. Performance of approximate exchange-correlation kernels in TDDFT for stoichiometric LN. With a common scissors shift of $\Delta = 2.0$ eV, the dielectric functions obtained with LRC ($\alpha = 0.75$) and the BO and RBO variants of the bootstrap kernel are mutually similar but deviate from the BSE results from Ref. [11] in terms of the peak positions and spectral weights. A reduced scissors shift of 1.4 eV and $\alpha = 0.44$ lead to very good quantitative agreement, however.

a rather similar impact on the dielectric function. Indeed, Fig. 2 illustrates that the LRC yields results close to both BO and RBO for stoichiometric LN if we set $\alpha = 0.75$ in accordance with the fit formula from [15] and apply a scissors shift of 2.0 eV in all cases. This value equals the self-energy correction of the fundamental indirect band gap of SLN [12] obtained with the quasiparticle self-consistent GW_0 (QSGW_0) approximation on top of Perdew-Burke-Ernzerhof (PBE), which is closely related to the PBEsol functional employed in this work, and is the same as in the BSE calculations by Riefer *et al.* [12] that we include as a benchmark in Fig. 2. The broadening of 0.15 eV is also identical in all calculations. Compared to the BSE results, all three TDDFT curves are blueshifted and exhibit incorrect oscillator strengths, however. The reason for this discrepancy is that the static LRC merely redistributes oscillator strength between existing peaks but does not shift the excitation energies themselves [15], a limitation shared by the BO and the RBO kernel. While this is inconsequential for standard sp^3-bonded semiconductors with weakly bound excitons, it causes problems in materials like LN, where the optical gap deviates significantly from the electronic band gap. In order to compensate for this deficiency, we treat the component of the exchange-correlation kernel associated with the quasiparticle shifts only partially as an explicit shift in $\chi^{\mathrm{KS}}_{\mathbf{GG}'}(\mathbf{q},\omega)$ and partially as a contribution to $f^{\mathrm{xc}}_{\mathbf{G}}(\mathbf{q})$, where it introduces a term analogous to (1) but with a positive prefactor [13–15]. Thereby, this manipulation simultaneously reduces the scissors shift and the parameter α in the LRC. Indeed, Fig. 2 shows that a scissors shift of 1.4 eV together with $\alpha = 0.44$ yields very good agreement with the BSE results, which in turn accurately reproduces the experimentally measured spectra [28,29], in terms of peak positions and spectral weights. Based on this quantitative calibration, we use the LRC with the same computational parameters not only for stoichiometric, but also for congruent and titanium-indiffused LN in the following.

The TDDFT calculations using the LRC are performed with YAMBO [30]. For defect-free stoichiometric LN simulated with one unit cell containing ten atoms, we use 350 electronic bands, 1500 reciprocal lattice vectors, and $6 \times 6 \times 6$ Γ-centered $\mathbf{k}$ points to obtain highly converged optical functions. To restrict the computational cost, we include 640 bands and 2700 $\mathbf{G}$ vectors for the $2 \times 2 \times 2$ supercell, whereas 1620 bands and 4000 $\mathbf{G}$ vectors are used for the $3 \times 3 \times 3$ supercell, with the same number of $\mathbf{k}$ points as in the corresponding ground-state calculations, albeit in a Γ-centered arrangement. This leads to a numerical error below 1.0% for the imaginary part of the dielectric function and the refractive index and below 1.5% for the real part of the dielectric function and the reflectivity in the case of the 80-atom supercell. For the larger 270-atom supercell, these values are below 1.5% and 3.3%, respectively. The calculations with the bootstrap kernel make use of the implementation in ELK [31]. By using identical lattice parameters and, where possible, the same computational parameters, we ensure that the results from the two codes are indeed comparable.

The frequency-dependent refractive index $n(\omega)$ and the extinction coefficient $\kappa(\omega)$ analyzed below are related to the macroscopic dielectric function according to

$$n(\omega) = \left(\frac{|\varepsilon(\omega)| + \mathrm{Re}\,\varepsilon(\omega)}{2} \right)^{1/2} \tag{4}$$

and

$$\kappa(\omega) = \left(\frac{|\varepsilon(\omega)| - \mathrm{Re}\,\varepsilon(\omega)}{2} \right)^{1/2} . \tag{5}$$

Finally, the reflectivity is given by

$$R(\omega) = \frac{[n(\omega) - 1]^2 + \kappa(\omega)^2}{[n(\omega) + 1]^2 + \kappa(\omega)^2} . \tag{6}$$

III. RESULTS

A. Atomic and electronic structure

Lithium niobate is a noncentrosymmetric trigonal crystal with the space group $R3c$. Here we use a hexagonal unit cell. The relaxation of the cell geometry leads to lattice constants $a = 5.133$ Å and $c = 13.828$ Å, which are in excellent agreement with the experimental data of Boysen and Altorfer [32] at room temperature (deviation −0.35%). These lattice parameters are then fixed for all subsequent calculations. In the case of systems containing point defects, only minor changes of the relative atomic positions surrounding the defects are observed as a result of the atomic relaxation between the $2 \times 2 \times 2$ and the $3 \times 3 \times 3$ supercells. Our results are presented in Table I. Overall, we find that the titanium substitutional disturbs the lattice only locally: The bond length from the defect site to the neighboring oxygen atoms is reduced by 7% and to the nearest niobium atom by 2% with respect to the stoichiometric configuration. Beyond a distance of 3.1 Å, the atoms are only marginally affected. An illustration of the local displacements is given in Fig. 3.

TABLE I. Calculated bond lengths between Li (SLN) or the Ti_{Li} substitutionals (Ti:SLN) and neighboring atoms in angstroms. For pristine SLN, experimental data are available for comparison. For Ti:SLN, we display results for two different supercell sizes. The symbols $O_\downarrow$ and $Nb_\downarrow$ indicate oxygen and niobium atoms below the Li or Ti_{Li} site, $O_\uparrow$ and $Nb_\uparrow$ those above.

SLN	Li–$O_\downarrow$	Li–$O_\uparrow$	Li–$Nb_\downarrow$	Li–$Nb_\uparrow$
This work	2.050	2.238	3.905	3.009
Expt.[a]	2.070	2.239	3.923	3.010
Ti:SLN	Ti_{Li}–$O_\downarrow$	Ti_{Li}–$O_\uparrow$	Ti_{Li}–$Nb_\downarrow$	Ti_{Li}–$Nb_\uparrow$
$2 \times 2 \times 2$	1.928	2.056	3.982	3.012
$3 \times 3 \times 3$	1.922	2.052	3.986	3.004

[a]Reference [32].

The electronic band structure of Ti:SLN is displayed in Fig. 4. The *d* states of titanium split due to the noncentrosymmetric position inside the octahedral field, similar as described by Sanson *et al.* [33] for iron substitutionals. The incorporation of one Ti atom per supercell thus gives rise to three additional empty bands near the conduction-band minimum, one with a_1 symmetry and two with *e* symmetry. Our results show that the defect states of titanium are resonant with the conduction bands, which explains the experimental findings that titanium impurities do not introduce absorption bands in LN waveguides [1,34]. The indirect electronic band gap of stoichiometric LN, 3.52 eV within the approximations used here, is reduced to 3.33 eV in titanium-indiffused Ti:SLN (see Fig. 4). Incidentally, this is almost identical to the value 3.31 eV determined for CLN with a Nb_{Li} antisite defect in the same $2 \times 2 \times 2$ supercell, corresponding to a Li:Nb ratio of 88%. For Ti:CLN with the highest concentration of titanium impurities considered in this work, 1.16×10^{21} atoms per cm^3, the band gap decreases slightly further to 3.28 eV. However, we obtain a value that is even smaller by 0.2 eV for the configuration with a larger Li:Nb ratio of 96% and a titanium concentration of 1.05×10^{21} atoms per cm^3. We attribute this to the different atomic arrangement and the resulting strong interaction between the different defect types, which are situated in neighboring unit cells along the *c* axis.

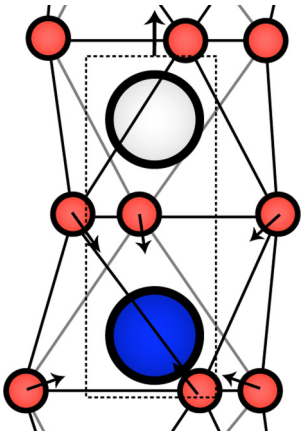

FIG. 3. Zoom into Fig. 1(b) with arrows indicating local atomic displacements due to the Ti_{Li} substitutional. Compared with the stoichiometric configuration, the niobium and titanium atoms are shifted upwards as indicated, while the oxygen atoms move towards the titanium site.

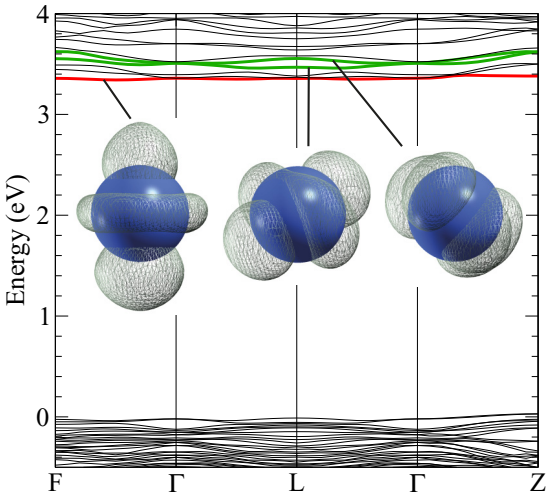

FIG. 4. Calculated electronic band structure of the Ti:SLN $2 \times 2 \times 2$ supercell. The titanium-related bands are highlighted in red (a_1 symmetry) and green (*e* symmetry). Inset pictures show the charge density (gray) around the Ti atom (blue) corresponding to the Kohn-Sham orbital of the localized defect state at selected points in the Brillouin zone.

We note that the calculated absolute values underestimate the experimental band gaps, a well-known feature of density-functional theory with semilocal exchange-correlation functionals like PBEsol. However, the relative changes due to structural or compositional modifications are typically reliable. Accurate quantitative calculations of electronic band gaps are possible within the *GW* approximation and have been reported for SLN [12,35], but at a much higher computational cost. In the following, the effect of the *GW* self-energy correction is simulated by a simple scissors operator that opens the band gap to an appropriate value.

B. Dielectric functions

Our calculated results for the imaginary part of the dielectric function are displayed in Fig. 5. We observe that the fine structure of the main absorption peak is largely washed out upon Ti indiffusion, as reported earlier by Li *et al.* [36] for CLN when compared to SLN. In addition, the onset of the main absorption at about 5 eV is shifted to lower energies, which results from the downshift of the conduction bands due to the Ti indiffusion.

In the case of SLN, it is interesting to note that the optical absorption is not a monotonous function of the Ti concentration: For energies inside the band gap, magnified in the insets of Fig. 5, the dielectric function initially decreases if titanium atoms are introduced into the material. However, as the titanium concentration becomes larger, it increases again.

Without indiffused titanium atoms, CLN exhibits a lower absorption than SLN inside the band gap, as the intrinsic defects reduce the imaginary part of the dielectric function. On the other hand, a growing concentration of Ti_{Li} substitutionals

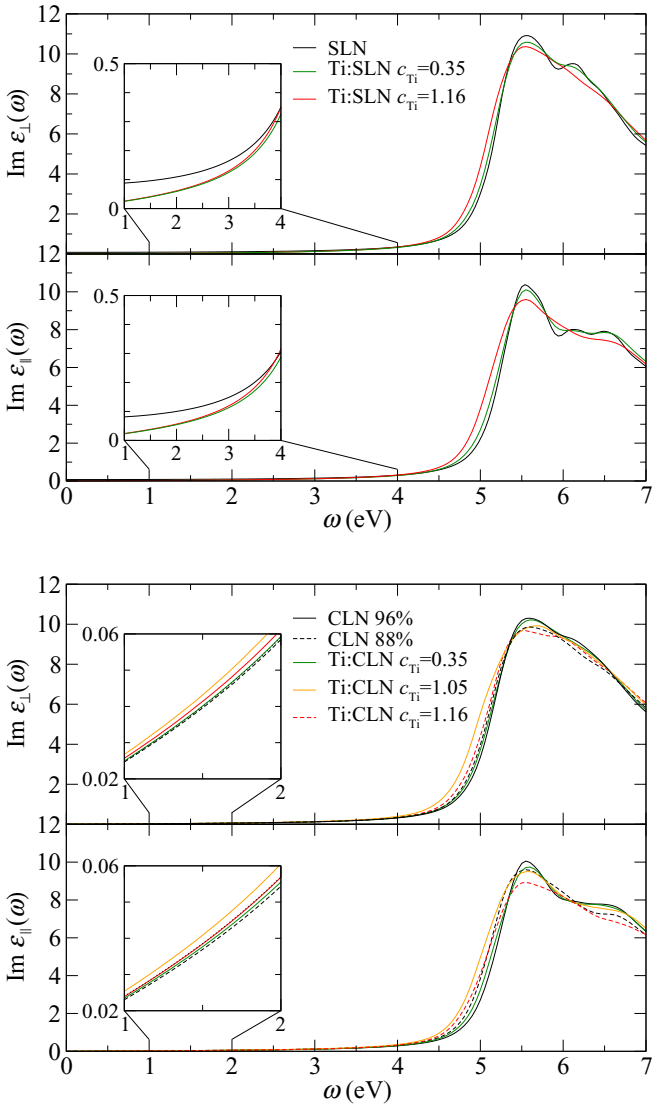

FIG. 5. Imaginary part of the dielectric functions for concentrations of 0.35, 1.05 (only CLN), and 1.16×10^{21} titanium atoms per cm^3 in stoichiometric (upper panel) and congruent (lower panel) lithium niobate. The components for electric fields perpendicular ($\perp$) and parallel ($\parallel$) to the c axis are shown separately. For CLN, the curves for 0.35 and 1.05×10^{21} Ti atoms per cm^3 correspond to a Li:Nb ratio of 96% and are obtained with the $3 \times 3 \times 3$ supercell, while those for 1.16×10^{21} Ti atoms per cm^3 correspond to a lower Li:Nb ratio of 88% and are obtained with the $2 \times 2 \times 2$ supercell.

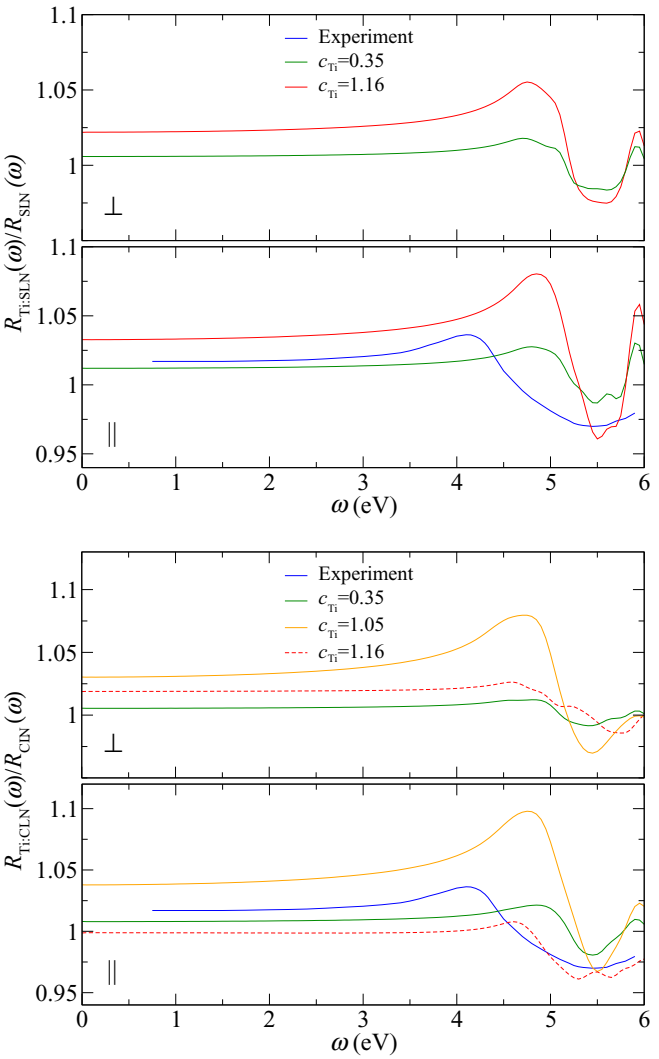

FIG. 6. Relative reflectivity $R_{\text{Ti:SLN}}/R_{\text{SLN}}$ and $R_{\text{Ti:CLN}}/R_{\text{CLN}}$ compared to experimental data from Ref. [34] for CLN with an unknown titanium concentration c_{Ti} between 0.1 and 1.5. The components for electric fields perpendicular ($\perp$) and parallel ($\parallel$) to the c axis are shown separately. For information about the impurity concentrations and Li:Nb ratios of the studied systems, see the caption of Fig. 5.

increases the absorption. This effect is more pronounced for the extraordinary component Im $\varepsilon_\parallel(\omega)$ and related to the internal electric field parallel to the c axis, which interacts with the incident light; note that LN is a birefringent material. The increasing impurity concentration disturbs this field and thereby modifies the absorption properties of the crystal.

C. Reflectivity

Unfortunately, there are few experimental data for the reflectivity of titanium-doped LN that can be directly compared with our theoretical predictions. Lüdtke and co-workers [34] measured the relative changes of the reflectivity perpendicular to the c axis with respect to congruent LN, i.e., the ratio $R_{\text{Ti:CLN}}(\omega)/R_{\text{CLN}}(\omega)$, for a sample with an unknown impurity concentration between 0.1 and 1.5×10^{21} Ti atoms per cm^3. In Fig. 6 we display the available experimental data together with our own results for $R_{\text{Ti:SLN}}(\omega)/R_{\text{SLN}}(\omega)$ and $R_{\text{Ti:CLN}}(\omega)/R_{\text{CLN}}(\omega)$ with comparable defect concentrations. To avoid inconsistencies in the quotient, we use the same convergence parameters for the reference reflectivity $R_{\text{SLN}}(\omega)$ as for the respective $R_{\text{Ti:SLN}}(\omega)$ for each configuration.

The qualitative characteristics of the experimental curve are evidently well reproduced. The most notable feature is the peak of the relative reflectivity between 4.5 and 5 eV. It is related to the reduction of the band gap with increasing impurity concentration in the material, as already noted above in connection with the dielectric function. Therefore, this peak is not a direct signature of the titanium dopants but an indirect effect, and its position depends on the impurity

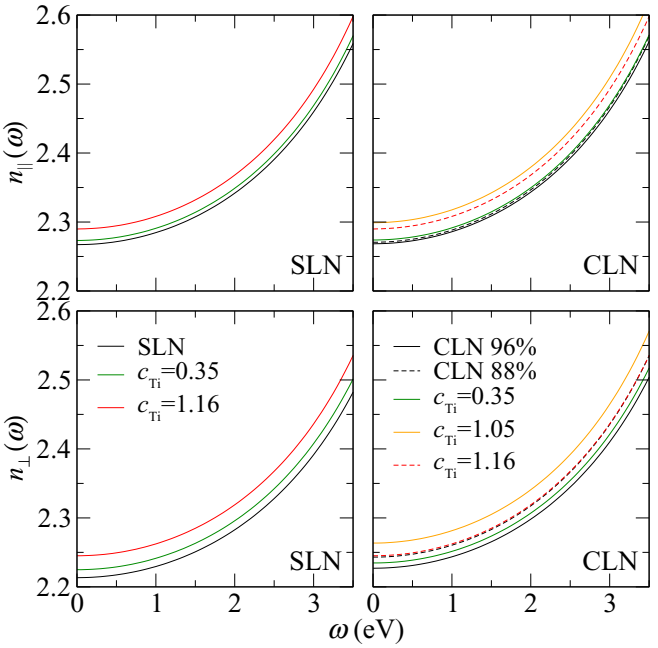

FIG. 7. Refractive indices $n(\omega)$ of stoichiometric and congruent LN with different titanium concentrations. The extraordinary $n_{\parallel}$ and ordinary $n_{\perp}$ components of the refractive indices are shown separately. For information about the impurity concentrations and Li:Nb ratios of the studied systems see the caption of Fig. 5.

concentration: For an increasing number of impurities, the peak shifts to lower energies. Furthermore, the magnitude of the reflectivity also depends on the impurity concentration. It is determined by the number of additional electronic states resonant with the conduction bands and therefore increases with the impurity concentration. A notable deviation from this behavior is observed for the reflectivity parallel to the ferroelectric axis in the case of a high concentration of both intrinsic and extrinsic defects. In particular, for Ti:CLN in the $2 \times 2 \times 2$ supercell with $c_{Ti} = 1.16$, the Ti_{Li} and Nb_{Li} substitutionals are situated in neighboring unit cells along the c axis, which strongly affects the internal electric field and hence the optical functions in this direction.

D. Refractive indices

According to experimental measurements, titanium doping of LN induces absolute changes in the refractive indices in the range of 10^{-3}–10^{-2} [1,34], which falls below the numerical accuracy that we can achieve for the large supercells required to simulate defects. However, we find that the convergence behavior in the frequency range of 0–4 eV is nearly identical for all systems studied here. Therefore, a significant error reduction can be achieved by determining the convergence offsets, i.e., the difference between the highly converged refractive indices and their underconverged counterparts, for the small defect-free unit cell of SLN and subsequently adding these to the approximate results obtained for other configurations. In this way, refractive indices initially calculated with different convergence parameters become directly comparable.

Our calculated refractive indices are shown in Fig. 7. We point out again that for congruent LN, we consider

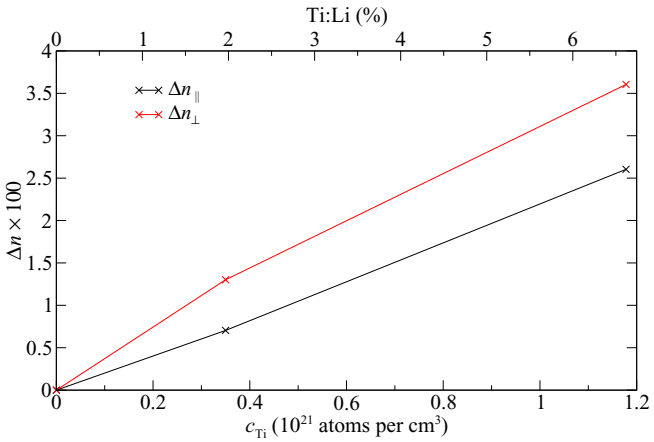

FIG. 8. Variation $\Delta n = n_{Ti:SLN} - n_{SLN}$ of the ordinary ($\perp$) and extraordinary ($\parallel$) refractive index at a wavelength of 630 nm (1.97 eV) as a function of the titanium concentration c_{Ti}, given in units of 10^{21} atoms per cm^3. The calculated data points are joined by lines to guide the eye.

configurations where titanium impurities are introduced in materials with different Li:Nb ratios, i.e., 88% for calculations using the 80-atom supercell and 96% for those using the 270-atom supercell. This must be borne in mind when comparing the reflective indices of Ti:CLN, especially for the ordinary refractive index $n_{\perp}(\omega)$. Similar to the findings for the reflectivity above, an increasing concentration of titanium impurities generally increases the magnitude of $n_{\perp}(\omega)$, but a high concentration of both Nb_{Li} antisites and Ti_{Li} substitutionals reverses this effect, as can be seen for Ti:CLN with $c_{Ti} = 1.16$, because the different defects are situated close to each other and affect the internal electric field.

Experimental measurements at a wavelength of 630 nm (1.97 eV) reveal that the extraordinary refractive index increases linearly with the titanium concentration, while the ordinary refractive index is a concave but monotonically increasing curve [1,34]. The calculated variations as a function of concentration are displayed in Fig. 8, which contains results for only Ti:SLN in order to exclude the influence of different Nb:Li ratios associated with the differently sized supercells used for congruent LN. Our findings are in accordance with the experimental data. The extraordinary refractive index increases linearly with the Ti concentration, while the ordinary refractive index exhibits a subtle concave bent. This is no numerical artifact of our calculations and can also be observed for Ti:CLN with a fixed Li:Nb ratio and a varying Ti concentration, as deduced from Fig. 7. Evidently, the increasing defect-defect interaction renders the influence of the titanium impurities on $n_{\perp}(\omega)$ less effective.

The increase of the refractive indices arises from the lattice distortion around the titanium substitutionals. Resubstituting lithium atoms on the titanium sites while retaining the atomic positions in the calculations of the refractive indices yields the same trend as found for Ti defects. This shows that the induced changes of the optical properties are not caused by the titanium atoms themselves but occur indirectly through the lattice deformation. Indeed, the electron density associated with the titanium orbitals is well localized at the titanium sites, as already discussed in relation with Fig. 4. We take this as

evidence that the Ti states strongly resemble atomic orbitals and scarcely hybridize with the host states.

IV. CONCLUSIONS

We have modeled the Ti doping in LN by means of DFT+U and TDDFT calculations using supercells with 80 and 270 atoms. We simulated different point-defect concentrations of Ti_{Li} substitutionals and Nb_{Li} antisite defects. The titanium atom on a lithium site can explain all available optical measurements. In particular, we find that the reflectivity and refractive indices are enhanced by increasing the titanium concentration, unless interactions between different defect types in the congruent material become dominant.

We trace the Ti-induced modification of the optical properties of LN to the local strain exerted by the impurities on the host lattice. Furthermore, our results show that the electronic states of the substitutionals are localized and exhibit only a small hybridization with the host states. This suggests that dopants other than Ti, which are inert and cause a large strain in the LN matrix, may be equally well, or possibly even better suited to realize LN waveguide structures.

ACKNOWLEDGMENTS

We thank H. Suche for useful discussions in the course of this work. All calculations were performed at the Paderborn Center for Parallel Computing (PC^2). We gratefully acknowledge financial support by the Deutsche Forschungsgemeinschaft (DFG) via Sonderforschungsbereich TRR 142, Project B04.

[1] M. Minakata, S. Saito, M. Shibata, and S. Miyazawa, J. Appl. Phys. **49**, 4677 (1978).
[2] G. Corradi, I. M. Zaritskii, A. Hofstaetter, K. Polgar, and L. G. Rakitina, Phys. Rev. B **58**, 8329 (1998).
[3] H. Söthe and J.-M. Spaeth, J. Phys.: Condens. Matter **4**, 9901 (1992).
[4] C. Zaldo, C. Prieto, H. Dexpert, and P. Fessler, J. Phys.: Condens. Matter **3**, 4135 (1991).
[5] H. Donnerberg, S. M. Tomlinson, C. R. A. Catlow, and O. F. Schirmer, Phys. Rev. B **40**, 11909 (1989).
[6] H. H. Nahm and C. H. Park, Phys. Rev. B **78**, 184108 (2008).
[7] H. Xu, D. Lee, J. He, S. B. Sinnott, V. Gopalan, V. Dierolf, and S. R. Phillpot, Phys. Rev. B **78**, 174103 (2008).
[8] H. Xu, A. Chernatynskiy, D. Lee, S. B. Sinnott, V. Gopalan, V. Dierolf, and S. R. Phillpot, Phys. Rev. B **82**, 184109 (2010).
[9] O. F. Schirmer, M. Imlau, C. Merschjann, and B. Schoke, J. Phys.: Condens. Matter **21**, 123201 (2009).
[10] P. Skeath, W. T. Elam, W. K. Burns, F. A. Stevie, and T. H. Briggs, Phys. Rev. Lett. **59**, 1950 (1987).
[11] A. Riefer, S. Sanna, A. Schindlmayr, and W. G. Schmidt, Phys. Rev. B **87**, 195208 (2013).
[12] A. Riefer, M. Friedrich, S. Sanna, U. Gerstmann, A. Schindlmayr, and W. G. Schmidt, Phys. Rev. B **93**, 075205 (2016).
[13] S. Botti, A. Schindlmayr, R. Del Sole, and L. Reining, Rep. Prog. Phys. **70**, 357 (2007).
[14] L. Reining, V. Olevano, A. Rubio, and G. Onida, Phys. Rev. Lett. **88**, 066404 (2002).
[15] S. Botti, F. Sottile, N. Vast, V. Olevano, L. Reining, H.-C. Weissker, A. Rubio, G. Onida, R. Del Sole, and R. W. Godby, Phys. Rev. B **69**, 155112 (2004).
[16] S. Sharma, J. K. Dewhurst, A. Sanna, and E. K. U. Gross, Phys. Rev. Lett. **107**, 186401 (2011).
[17] S. Rigamonti, S. Botti, V. Veniard, C. Draxl, L. Reining, and F. Sottile, Phys. Rev. Lett. **114**, 146402 (2015).
[18] J. A. Berger, Phys. Rev. Lett. **115**, 137402 (2015).
[19] S. C. Abrahams and P. Marsh, Acta Crystallogr., Sect. B: Struct. Sci. **42**, 61 (1986).
[20] P. Giannozzi, S. Baroni, N. Bonini, M. Calandra, R. Car, C. Cavazzoni, D. Ceresoli, G. L. Chiarotti, M. Cococcioni, I. Dabo, A. Dal Corso, S. de Gironcoli, S. Fabris, G. Fratesi, R. Gebauer, U. Gerstmann, C. Gougoussis, A. Kokalj, M. Lazzeri, L. Martin-Samos, N. Marzari, F. Mauri, R. Mazzarello, S. Paolini, A. Pasquarello, L. Paulatto, C. Sbraccia, S. Scandolo, G. Sclauzero, A. P. Seitsonen, A. Smogunov, P. Umari, and R. M. Wentzcovitch, J. Phys.: Condens. Matter **21**, 395502 (2009).
[21] J. P. Perdew, A. Ruzsinszky, G. I. Csonka, O. A. Vydrov, G. E. Scuseria, L. A. Constantin, X. Zhou, and K. Burke, Phys. Rev. Lett. **100**, 136406 (2008).
[22] M. Friedrich, A. Riefer, S. Sanna, W. G. Schmidt, and A. Schindlmayr, J. Phys.: Condens. Matter **27**, 385402 (2015).
[23] M. Friedrich, A. Schindlmayr, W. G. Schmidt, and S. Sanna, Phys. Status Solidi B **253**, 683 (2016).
[24] F. Schmidt, M. Landmann, E. Rauls, N. Argiolas, S. Sanna, W. G. Schmidt, and A. Schindlmayr, Adv. Mater. Sci. Eng. **2017**, 3981317 (2017).
[25] D. R. Hamann, Phys. Rev. B **88**, 085117 (2013).
[26] H. J. Monkhorst and J. D. Pack, Phys. Rev. B **13**, 5188 (1976).
[27] M. Cococcioni and S. de Gironcoli, Phys. Rev. B **71**, 035105 (2005).
[28] E. Wiesendanger and G. Güntherodt, Solid State Commun. **14**, 303 (1974).
[29] A. M. Mamedov, M. A. Osman, and L. C. Hajieva, Appl. Phys. A: Solids Surf. **34**, 189 (1984).
[30] A. Marini, C. Hogan, M. Grüning, and D. Varsano, Comput. Phys. Commun. **180**, 1392 (2009).
[31] http://elk.sourceforge.net (2004).
[32] H. Boysen and F. Altorfer, Acta Crystallogr., Sect. B: Struct. Sci. **50**, 405 (1994).
[33] A. Sanson, A. Zaltron, N. Argiolas, C. Sada, M. Bazzan, W. G. Schmidt, and S. Sanna, Phys. Rev. B **91**, 094109 (2015).
[34] H. Lüdtke, W. Sohler, and H. Suche, in *Dig. Workshop Integrated Optics*, edited by R. T. Kersten and R. Ulrich (Technische Universität Berlin, Berlin, 1980), pp. 122–126.
[35] C. Thierfelder, S. Sanna, A. Schindlmayr, and W. G. Schmidt, Phys. Status Solidi C **7**, 362 (2010).
[36] Y. Li, W. G. Schmidt, and S. Sanna, Phys. Rev. B **91**, 174106 (2015).